J. Fluid Mech. (2019), *vol.* 868, R5, doi:10.1017/jfm.2019.227

JFM RAPIDS
journals.cambridge.org/rapids

The instability of gyrotactically trapped cell layers

Smitha Maretvadakethope[1], Eric E. Keaveny[1] and Yongyun Hwang[2,†]

[1]Department of Mathematics, Imperial College London, South Kensington, London SW7 2AZ, UK

[2]Department of Aeronautics, Imperial College London, South Kensington, London SW7 2AZ, UK

(Received 29 November 2018; revised 13 February 2019; accepted 18 March 2019)

Several metres below the coastal ocean surface there are areas of high ecological activity that contain thin layers of concentrated motile phytoplankton. Gyrotactic trapping has been proposed as a potential mechanism for layer formation of bottom-heavy swimming algae cells, especially in flows where the vorticity varies linearly with depth (Durham *et al.*, *Science*, vol. 323(5917), 2009, pp. 1067–1070). Using a continuum model for dilute microswimmer suspensions, we report that an instability of a gyrotactically trapped cell layer can arise in a pressure-driven plane channel flow. The linear stability analysis reveals that the equilibrium cell-layer solution is hydrodynamically unstable due to negative microswimmer buoyancy (i.e. a gravitational instability) over a range of biologically relevant parameter values. The critical cell concentration for this instability is found to be $N_c \simeq 10^4$ cells cm^{-3}, a value comparable to the typical maximum cell concentration observed in thin layers. This result indicates that the instability may be a potential mechanism for limiting the layer's maximum cell concentration, especially in regions where turbulence is weak, and motivates the study of its nonlinear evolution, perhaps, in the presence of turbulence.

Key words: bioconvection

1. Introduction

Oceanographic studies have shown that near coastal regions long and thin layers of phytoplankton form several metres beneath the surface and persist for days (Nielsen, Kiørboe & Bjørnsen 1990; Dekshenieks *et al.* 2001; Stacey, McManus & Steinbuck 2007; Sullivan, Donaghay & Rines 2010). These layers have cell concentrations orders of magnitude higher than ambient values (Sullivan *et al.* 2010) and are ecological hot spots that significantly contribute to species diversity in marine environments (Grünbaum 2009). Their thickness ranges from a few centimetres to

† Email address for correspondence: y.hwang@imperial.ac.uk

© Cambridge University Press 2019

Downloaded from https://www.cambridge.org/core. Imperial College London Library, on 15 Apr 2019 at 13:41:41, subject to the Cambridge Core terms of use, available at https://www.cambridge.org/core/terms. https://doi.org/10.1017/jfm.2019.227

a few metres and they can extend horizontally for kilometres (Dekshenieks *et al.* 2001; Moline *et al.* 2010). These layers often emerge in areas where turbulence is considerably weak or highly suppressed by surrounding flow conditions (e.g. density stratification) (Dekshenieks *et al.* 2001). A number of mechanisms have been proposed for layer formation, and they include convergent swimming originating from 'taxes' of motile phytoplankton (MacIntyre, Cullen & Cembella 1997; Grünbaum 2009; Ryan, McManus & Sullivan 2010), vertical stratification in oceans, especially at pycnoclines (Dekshenieks *et al.* 2001; Johnston & Rudnick 2009), straining by shear (Franks 1995; Osborn 1998; Stacey *et al.* 2007) and gyrotactic trapping (Durham, Kessler & Stocker 2009). The reader may refer to Durham & Stocker (2012) for a review on this issue.

Of particular interest to the present study is the mechanism of gyrotactic trapping, which has been proposed for green algae, like those of genus *Chlamydomonas* or *Dunaliella* (Durham *et al.* 2009). These microorganisms are commonly observed in lakes, seas and oceans (Ginzburg & Ginzburg 1985; Similä 1988; Krivtsov, Bellinger & Sigee 2000) and they exhibit sensitivity to gravity (Kessler 1984). This is the consequence of bottom heaviness originating from the fact that the centre of mass of the cell is displaced from that of buoyancy. This displacement results in a gravitational torque causing the cell to swim upwards (Kessler 1985). In the presence of shear, however, such a cell also experiences a viscous torque due to the vorticity of the flow, and the swimming direction is then determined by the balance between the gravitational and viscous torques (i.e. gyrotaxis). In particular, if the shear is very large, the cell continuously tumbles (Pedley & Kessler 1987) and gradually loses its upswimming velocity on average.

Durham *et al.* (2009) proposed that an excessively large shear (or vorticity) disrupts the upswimming of large numbers of gyrotactic cells, thereby leading to the formation of a thin layer in the region of large shear (i.e. gyrotactic trapping). To demonstrate this mechanism, they performed a laboratory experiment where a flow with an approximately linearly growing shear rate is applied to a suspension of gyrotactic cells (*Chlamydomonas nivalis* and *Heterosigma akashiwo*) with 1 cm depth. It was shown that a thin layer of cells is indeed formed by the proposed mechanism. However, the layer was also found to be highly unsteady and exhibit non-trivial dynamics in the sense that the formation of the layer is highly transient (see also the numerical study by Santamaria *et al.* 2014), even though the background flow itself remained laminar and steady (private communication with W. M. Durham). In bioconvection, a thin layer is formed at the upper fluid boundary due to the upswimming of the cells. This layer has been found to become unstable as the high cell concentration causes gravitational overturning, which in turn causes a convection pattern to arise (see, for example, Pedley, Hill & Kessler 1988; Pedley & Kessler 1992; Bees & Hill 1997). Similarly, the thin layers formed in the suspension by gyrotactic trapping are suspected to exhibit a similar instability, which may explain the highly unsteady layer dynamics observed in experiments.

The objective of the present study is to examine the stability of layers formed by gyrotactic trapping using the continuum model described in Pedley (2010) and Hwang & Pedley (2014*a*). To this end, we consider a suspension of gyrotactic microorganisms subject to a horizontal plane Poiseuille flow which has a shear rate (or vorticity) that grows linearly in the vertical direction, as in the experiments by Durham *et al.* (2009). To some extent, this flow configuration appears to be similar to that of the experiment by Croze, Ashraf & Bees (2010) in which a horizontal pipe Poiseuille flow was applied to a suspension of *C. augustae*. However, unlike the pipe flow, the shear

Downloaded from https://www.cambridge.org/core. Imperial College London Library, on 15 Apr 2019 at 13:41:41, subject to the Cambridge Core terms of use, available at https://www.cambridge.org/core/terms. https://doi.org/10.1017/jfm.2019.227

in horizontal plane Poiseuille flow is purely vertical, and we will see that this flow geometry admits a steady equilibrium solution in the form of a gyrotactically trapped cell layer. This is the important physical feature which distinguishes the present study from the work by Croze *et al.* (2010) as well as the one by Hwang & Pedley (2014*a*) which studied the role of uniform shear in bioconvection: the pressure-driven channel flow has an equilibrium solution corresponding to a gyrotactically trapped cell layer whose stability can then be assessed. Finally, it is worth mentioning that the layer formation in the plane Poiseuille flow of gyrotactic microorganism suspensions is reminiscent of that found for bacterial suspensions in a microfluidic channel (Rusconi, Guasto & Stocker 2014). However, the underlying mechanism for the layer formation between the two cases is fundamentally different.

2. Problem formulation

2.1. *Equations of motion*

The mathematical model and its stability analysis in the present study are based on those described in Hwang & Pedley (2014*a*). This model is derived from the Navier–Stokes equations combined with a Smoluchowski equation describing the cell distribution in time, space and cell-orientation space. The model adopts the translational diffusivity expression proposed by Pedley & Kessler (1990), although this can be improved by the generalised Taylor's dispersion theory (for example, Hill & Bees 2002). In our presentation here, we have omitted repeated details for brevity. Suppose we have a fluid of density, ρ, and kinematic viscosity, ν, in an infinitely long and infinitely wide channel, subject to a constant pressure gradient in the horizontal direction. Here, we denote x^*, y^* and z^* as the streamwise, vertical and spanwise directions, respectively, and t^* as the time (note that the superscript * denotes dimensional variables). The two walls of the channel are located at $y^* = \pm h$, where h is half-height of the channel. In this horizontal channel there is a suspension of spherical gyrotactic cells with average cell-number density, N. The individual cell is assumed to swim at speed V_c^* and is subject to gravity, as well as diffusion. The cell sedimentation speed is given by V_s^*, and, as we shall see in § 3.1, plays a crucial role in the formation of the gyrotactically trapped equilibrium layer. The swimming direction of the cells is denoted by a unit vector, $\boldsymbol{e} = (e_1, e_2, e_3)$, and their sedimentation direction is $-\boldsymbol{j}$ (where $\boldsymbol{j}$ is the upward unit vector in the vertical direction). As shown in Pedley & Kessler (1990), the translational diffusivity of the suspension scales like $V_c^{*2}\tau$, where τ is the swimming direction correlation time. We use this as the representative value for translational diffusivity, such that $D_V \equiv V_c^{*2}\tau$. Using the length scale h, the diffusion velocity scale D_V/h, and the average cell-number density N, the dimensionless equations of motion are:

$$\boldsymbol{\nabla}\cdot\boldsymbol{u} = 0, \tag{2.1a}$$

$$Sc^{-1}\left(\frac{\partial \boldsymbol{u}}{\partial t} + (\boldsymbol{u}\cdot\boldsymbol{\nabla})\boldsymbol{u}\right) = -\boldsymbol{\nabla}p + \nabla^2\boldsymbol{u} - Ra\ n\boldsymbol{j}, \tag{2.1b}$$

$$\frac{\partial n}{\partial t} + \boldsymbol{\nabla}\cdot[n(\boldsymbol{u} + V_c\langle\boldsymbol{e}\rangle - V_s\boldsymbol{j})] = \boldsymbol{\nabla}\cdot(\boldsymbol{D}_T\cdot\boldsymbol{\nabla}n), \tag{2.1c}$$

with the no-slip and no-flux boundary conditions on the walls

$$\boldsymbol{u}|_{y=\pm1} = (0, 0, 0), \tag{2.1d}$$

$$[n(\boldsymbol{u} + V_c\langle\boldsymbol{e}\rangle - V_s\boldsymbol{j}) - \boldsymbol{D}_T\cdot\boldsymbol{\nabla}n]|_{y=\pm1}\cdot\boldsymbol{j} = 0, \tag{2.1e}$$

Downloaded from https://www.cambridge.org/core. Imperial College London Library, on 15 Apr 2019 at 13:41:41, subject to the Cambridge Core terms of use, available at https://www.cambridge.org/core/terms. https://doi.org/10.1017/jfm.2019.227

where $\boldsymbol{u}(=(u, v, w))$, p, n, V_c, V_s and $\boldsymbol{D}_T$ ($\equiv \langle \boldsymbol{ee} \rangle - \langle \boldsymbol{e} \rangle \langle \boldsymbol{e} \rangle$; see also Pedley & Kessler (1990) for this expression), are the dimensionless velocity, pressure, cell-number density, cell-swimming speed, cell sedimentation speed, and translational diffusivity tensor, respectively. The Schmidt number Sc and the Rayleigh number Ra in (2.1*b*) are given by

$$Sc = \frac{\nu}{D_V} \quad \text{and} \quad Ra = \frac{N\upsilon g' h^3}{D_V \nu}, \tag{2.1f,g}$$

where $g' = g\Delta\rho/\rho$ is the reduced gravity ($\Delta\rho$ is the density difference between the cell and fluid) and υ the volume of a cell. In (2.1*c*) and (2.1*e*), $\langle \cdot \rangle$ denotes the local ensemble average at given spatial location $\boldsymbol{x}$, which is obtained with the p.d.f. of the cell-swimming orientation, $f(\boldsymbol{x}, \boldsymbol{e}, t)$. This satisfies

$$D_R^{-1} \frac{\partial f}{\partial t} + D_R^{-1} (\boldsymbol{u} \cdot \boldsymbol{\nabla}) f + \boldsymbol{\nabla}_e \cdot \left(\lambda (\boldsymbol{j} - (\boldsymbol{j} \cdot \boldsymbol{e}) \boldsymbol{e}) f + \frac{\boldsymbol{\Omega}}{2D_R} \times \boldsymbol{e} f \right) = \nabla_e^2 f, \tag{2.1h}$$

where $\boldsymbol{\Omega}$ is the flow vorticity. Here, the dimensionless rotational diffusivity D_R and the dimensionless inverse of the gyrotactic time scale λ are also given by

$$D_R \equiv \frac{D_R^* h^2}{D_V} \quad \text{and} \quad \lambda = \frac{1}{2BD_R^*}, \tag{2.1i,j}$$

with the rotational diffusivity D_R^* and the gyrotactic time scale B.

2.2. *Basic state*

Given the horizontal homogeneity of the flow, equation (2.1) admits the following equilibrium solution:

$$\boldsymbol{u}_0(y) = (U_0(y), 0, 0), \quad n = n_0(y), \tag{2.2a}$$

where

$$U_0(y) = ScRe(1 - y^2), \tag{2.2b}$$

$$n_0(y) = N_0 \exp\left(\int \frac{V_c \langle e_2 \rangle_0 - V_s}{D_{T0}^{22}} \mathrm{d}y \right). \tag{2.2c}$$

Here, $Re = U_c h/\nu$ is the Reynolds number based on the centreline velocity U_c, and N_0 is the normalisation constant setting the volume average of $n_0(y)$ to be unity. Also, in (2.2*c*), $\langle \cdot \rangle_0$ is obtained from the steady and horizontally uniform solution f_0 of (2.1*h*): i.e.

$$\boldsymbol{\nabla}_e \cdot \left(\lambda (\boldsymbol{j} - (\boldsymbol{j} \cdot \boldsymbol{e}) \boldsymbol{e}) f_0 + \frac{\boldsymbol{\Omega}_0}{2D_R} \times \boldsymbol{e} f_0 \right) = \nabla_e^2 f_0, \tag{2.2d}$$

where $\boldsymbol{\Omega}_0 = (0, 0, -ScRe(\mathrm{d}U_0/\mathrm{d}y))$.

In the regime of high shear rates, one may estimate the formation time scale of the basic state from an initially uniform suspension. In this case, the effect of the upswimming velocity would be negligible due to very high surrounding shear. Therefore, the time scale for layer formation will be given by the length scale of the system and translational diffusivity, such that

$$T_{layer} \sim \frac{h^2}{D_V^*} = \frac{(0.25)^2}{1.98 \times 10^{-4}} \approx 300 \text{ s}. \tag{2.3}$$

Downloaded from https://www.cambridge.org/core. Imperial College London Library, on 15 Apr 2019 at 13:41:41, subject to the Cambridge Core terms of use, available at https://www.cambridge.org/core/terms.
https://doi.org/10.1017/jfm.2019.227

2.3. *Linear stability analysis*

Now, let us consider a small perturbation around the basic state, such that: $[\boldsymbol{u}\ n\ f]^{\mathrm{T}} = [\boldsymbol{u}_0\ n_0\ f_0]^{\mathrm{T}} + \epsilon[\boldsymbol{u}'\ n'\ f']^{\mathrm{T}} + O(\epsilon^2)$ for $\epsilon \ll 1$. The normal-mode solution of the perturbation is then written as

$$[\boldsymbol{u}'\ n'\ f']^{\mathrm{T}}(x, y, z, t) = [\hat{\boldsymbol{u}}\ \hat{n}\ \hat{f}]^{\mathrm{T}} \mathrm{e}^{\mathrm{i}(\alpha x + \beta z - \omega t)} + \mathrm{c.c}, \tag{2.4}$$

where ω is the unknown complex angular frequency, and α and β are the given streamwise and spanwise wavenumbers, respectively. Using the standard procedure that eliminates pressure perturbation, the vertical velocity and vorticity form of the linearised equations of motion are given by

$$\mathrm{i}\omega \begin{pmatrix} Sc^{-1}(k^2 - \mathcal{D}^2) & 0 & 0 \\ 0 & Sc^{-1} & 0 \\ 0 & 0 & 1 \end{pmatrix} \begin{pmatrix} \hat{v} \\ \hat{\eta} \\ \hat{n} \end{pmatrix} = \begin{pmatrix} L_{OS} & 0 & k^2 Ra \\ \mathrm{i}\beta Re \mathcal{D}U & L_{SQ} & 0 \\ \mathcal{D}n_0 + L_C^v & L_C^\eta & L_C \end{pmatrix} \begin{pmatrix} \hat{v} \\ \hat{\eta} \\ \hat{n} \end{pmatrix}, \tag{2.5a}$$

where

$$L_{OS} = \mathrm{i}\alpha ReU(k^2 - \mathcal{D}^2) + \mathrm{i}\alpha Re\mathcal{D}^2 U + (k^2 - \mathcal{D}^2)^2, \tag{2.5b}$$

$$L_{SQ} = \mathrm{i}\alpha ReU + (k^2 - \mathcal{D}^2), \tag{2.5c}$$

$$\begin{aligned} L_C = {} & \mathrm{i}\alpha ScReU + \mathrm{i}\alpha V_c\langle e_1\rangle_0 + (V_c\langle e_2\rangle_0 - V_s)\mathcal{D} + \mathrm{i}\beta V_c\langle e_3\rangle_0 + V_c\mathcal{D}\langle e_2\rangle_0 \\ & + \alpha^2 D_{T0}^{11} - 2\mathrm{i}\alpha D_{T0}^{12}\mathcal{D} - D_{T0}^{22}\mathcal{D}^2 + \beta^2 D_{T0}^{33} - \mathrm{i}\alpha\mathcal{D}D_{T0}^{12} - \mathcal{D}D_{T0}^{22}\mathcal{D}, \end{aligned} \tag{2.5d}$$

$$\begin{aligned} L_C^v = {} & \left[G_1\mathcal{D}n_0\frac{\xi_2}{k^2}\mathrm{i}\alpha + n_0 G_1\left(-\alpha^2\frac{\xi_1}{k^2} + \mathcal{D}\xi_2\frac{\mathrm{i}\alpha}{k^2} + \frac{\xi_2}{k^2}\mathcal{D}\mathrm{i}\alpha + \beta^2\frac{\xi_3}{k^2}\right)\right. \\ & \left. - G_2\left(\mathrm{i}\alpha\frac{\xi_6}{k^2}\mathcal{D}^2 n_0 + \mathcal{D}n_0\left(-\alpha^2\frac{\xi_5}{k^2} + \mathcal{D}\xi_6 y\frac{\mathrm{i}\alpha}{k^2} + \frac{\xi_6}{k^2}\mathcal{D}\mathrm{i}\alpha + \beta^2\frac{\xi_7}{k^2}\right)\right)\right](k^2 - \mathcal{D}^2), \end{aligned} \tag{2.5e}$$

$$\begin{aligned} L_C^\eta = {} & G_1\mathcal{D}n_0\frac{\xi_2}{k^2}\mathrm{i}\beta\mathcal{D} + n_0 G_1\left[\left(\mathcal{D}\xi_2\frac{\mathrm{i}\beta}{k^2} + \frac{\xi_2}{k^2}\mathcal{D}\mathrm{i}\beta - \alpha\beta\frac{\xi_3}{k^2} - \alpha\beta\frac{\xi_1}{k^2}\right)\mathcal{D} + \xi_4\mathrm{i}\beta\right] \\ & - G_2\left[\mathcal{D}n_0\left(\xi_8\mathrm{i}\beta + \left(-\alpha\beta\frac{\xi_5}{k^2} + \frac{\mathrm{i}\beta}{k^2}\mathcal{D}\xi_6 + \frac{\xi_6}{k^2}\mathcal{D}\mathrm{i}\beta - \alpha\beta\frac{\xi_7}{k^2}\right)\mathcal{D}\right) + \mathrm{i}\beta\frac{\xi_6}{k^2}\mathcal{D}^2 n_0\mathcal{D}\right], \end{aligned} \tag{2.5f}$$

with the boundary conditions

$$\hat{v}|_{y=\pm1} = \mathcal{D}\hat{v}|_{y=\pm1} = \hat{\eta}|_{y=\pm1} = 0, \tag{2.5g}$$

$$\begin{aligned} & \left[\left(V_c\langle e_2\rangle_0 - V_s - \mathrm{i}\alpha D_{T0}^{12}\right)\hat{n} - D_{T0}^{22}\mathcal{D}\hat{n} + (G_1\xi_2 n_0 - G_2\xi_6\mathcal{D}n_0)\right. \\ & \left. \times\left(\frac{\mathrm{i}\alpha}{k^2}(k^2 - \mathcal{D}^2)\hat{v} + \frac{\mathrm{i}\beta}{k^2}\mathcal{D}\hat{\eta}\right)\right]_{y=\pm1} = 0. \end{aligned} \tag{2.5h}$$

Here, $\mathcal{D} = \mathrm{d}/\mathrm{d}y$, $k^2 = \alpha^2 + \beta^2$, $\hat{\eta} = \mathrm{i}\beta\hat{u} - \mathrm{i}\alpha\hat{w}$, and ξ_i are coefficients obtained in Hwang & Pedley (2014*a*) by applying a quasi-steady and quasi-uniform approximation to the linearised equation for f'. We note that this approximation would be valid as long as the instability does not carry a flow perturbation with very small time

Downloaded from https://www.cambridge.org/core. Imperial College London Library, on 15 Apr 2019 at 13:41:41, subject to the Cambridge Core terms of use, available at https://www.cambridge.org/core/terms. https://doi.org/10.1017/jfm.2019.227

Parameter	Description	Reference value
Sc	Schmidt number	50.39
Ra	Rayleigh number	10^0–10^4
G_1	See text	0.38
$G_2(=1/D_R)$	See text	0.05
λ	Inverse of dimensionless gyrotactic time scale	2.2
Re	Reynolds number of base-flow shear	0–6.28
S_{max}	Maximum shear rate normalised by D_R^*	0–30

TABLE 1. Dimensionless parameters in the present study.

and length scales (Hwang & Pedley 2014*a*). Fortunately, in laminar flows, such a perturbation would be damped by viscosity and diffusivity. In (2.5), $G_1 = V_c/D_R$ and $G_2 = 1/D_R$, and they indicate the relative importance of the cell-swimming velocity and translational diffusion to rotational diffusion, respectively.

The eigenvalue problem (2.5) is solved numerically by modifying the numerical solver used in Hwang & Pedley (2014*a*). Here, the derivatives in the vertical direction are discretised using a Chebyshev collocation method and, in the present study, all computations were carried out with 101 collocation points (i.e. $N_y = 101$). We also note that no discernible changes were found for several test cases when increasing to $N_y = 201$.

2.4. *Model parameters*

The depth of the channel in the present study is chosen to be $d(\equiv 2h) = 0.5$ cm, which is comparable to that used in Durham *et al.* (2009) ($d = 1$ cm). The range of the centreline velocity U_c tested in the present study is $U_c = 0$–0.25 cm s^{-1}, leading to $Re = 0$–6.28. The onset of gyrotactic trapping is strongly linked to the base-flow vorticity at which an isolated cell will begin to tumble. For a given dimensionless gyrotactic time scale λ, such a vorticity can be calculated either in terms of the gyrotactic time scale B or in terms of the rotational diffusivity D_R^*. The critical spanwise vorticity (made dimensionless by the rotational diffusivity) at which a cell undergoing no random motion begins to tumble is $S_{crit} = 4.4$, where the spanwise vorticity of the base flow is defined as

$$S(y) = -\frac{ScRe}{D_R^*}\frac{\mathrm{d}U_0}{\mathrm{d}y}. \tag{2.6}$$

We note that (2.6) is useful in characterising the flow rate in relation to the cell dynamics. Using (2.6), the base-flow rate can be characterised by the maximum spanwise vorticity,

$$S_{max} \equiv \max_y S(y), \tag{2.7}$$

for which $S(y) = S_{max}(= 2ScRe/D_R)$ is attained at the upper wall (i.e. $y = 1$).

All the model parameters for the individual cells in the present study (e.g. swimming speed, sedimentation speed, cell volume, etc) are those for *C. nivalis*. The range of the averaged cell-number density considered in the present study is $N = 1 \times 10^3$–1×10^7 cells cm^{-3}, which comfortably includes 1.1×10^6 cells cm^{-3} in the experiment of Durham *et al.* (2009). Given the flow geometry and the parameters for the cell, this results in $Ra = 10^0$–10^4. All the dimensionless parameters examined in the present study are summarised in table 1.

Downloaded from https://www.cambridge.org/core. Imperial College London Library, on 15 Apr 2019 at 13:41:41, subject to the Cambridge Core terms of use, available at https://www.cambridge.org/core/terms. https://doi.org/10.1017/jfm.2019.227

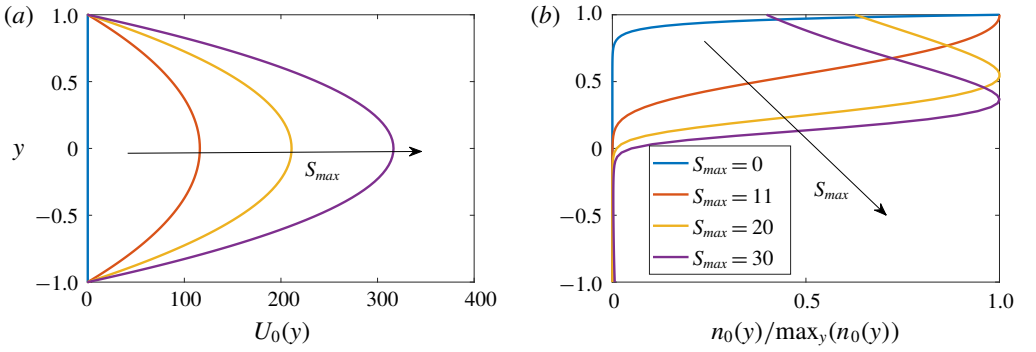

FIGURE 1. Profiles of the basic state with $S_{max} = 0$, 11, 20, 30: (*a*) base flow; (*b*) cell-number density normalised by its maximum.

3. Results and discussion

3.1. *Basic state*

The base flow and the corresponding cell-number density distribution are plotted in figure 1(*a,b*), respectively. As S_{max} is increased, the centreline velocity simply increases while maintaining the parabolic profile. In contrast, the profile of the cell-number density experiences non-trivial changes with the increase of S_{max}. To explain this feature, we start by making a few observations. First, for a excessively large spanwise vorticity, the average upswimming speed of the cells should become smaller than the sedimentation speed, because the upswimming speed $V_c\langle e_2\rangle_0$ approaches zero in the limit of infinitely large vorticity (see figure 3*a* in Hwang & Pedley 2014*a*). In other words, $V_c\langle e_2\rangle_0 \leqslant V_s$ for $S(y) \geqslant S_s$, where S_s is the spanwise vorticity at which $V_c\langle e_2\rangle_0 = V_s$. Note that, for the given modelling parameters, $S_s \simeq 11$ (figure 7 in Hwang & Pedley 2014*a*). Second, the form of $n_0(y)$ in (2.2*c*) indicates that the sign of $V_c\langle e_2\rangle_0 - V_s$ should be identical to that of $\mathrm{d}n_0/\mathrm{d}y$. It follows that the peak location of $n_0(y)$ is identical to the location where $S(y) = S_s$ (or equivalently $V_c\langle e_2\rangle_0 = V_s$), suggesting the crucial role of the sedimentation speed in the gyrotactic trapping even if it is significantly smaller than the cell-swimming speed (note that $V_s \simeq 0.1V_c$; see Pedley 2010).

Keeping these observations in mind, let us now observe $n_0(y)$ in figure 1(*b*) again. For $S_{max} = 0$, $n_0(y)$ is simply an exponentially growing function in the vertical direction because $\langle e_2\rangle_0$ and D_{T0}^{22} in (2.2*c*) are constant. When $S_{max} = 11$, $S(y = 1) \simeq S_s$. Therefore, $\mathrm{d}n_0/\mathrm{d}y \simeq 0$ at $y = 1$. If S_{max} is increased further ($S_{max} = 20$), the peak location of $n_0(y)$, at which $S(y) = S_s$, now emerges in the region of $0 < y < 1$, exhibiting an equilibrium layer of the cells formed by the gyrotactic trapping. With a further increase of S_{max}, the peak location of $n_0(y)$ is shifted further downwards, as is shown for $S_{max} = 30$.

3.2. *Linear stability analysis*

A linear stability analysis of the basic states in § 3.1 is now performed. The contours of the growth rate ω_i of the most unstable spanwise uniform ($\beta = 0$) mode in the Ra–α plane are shown in figure 2 for $S_{max} = 0$, 11, 20 and 30. For $S_{max} = 0$ (figure 2*a*), the neutral stability curve and the contour plot are identical to those for stationary bioconvection in Bees & Hill (1998) and Hwang & Pedley (2014*a*). On increasing S_{max}, the instabilities at high streamwise wavenumbers ($\alpha > 20$) are significantly

Downloaded from https://www.cambridge.org/core. Imperial College London Library, on 15 Apr 2019 at 13:41:41, subject to the Cambridge Core terms of use, available at https://www.cambridge.org/core/terms.
https://doi.org/10.1017/jfm.2019.227

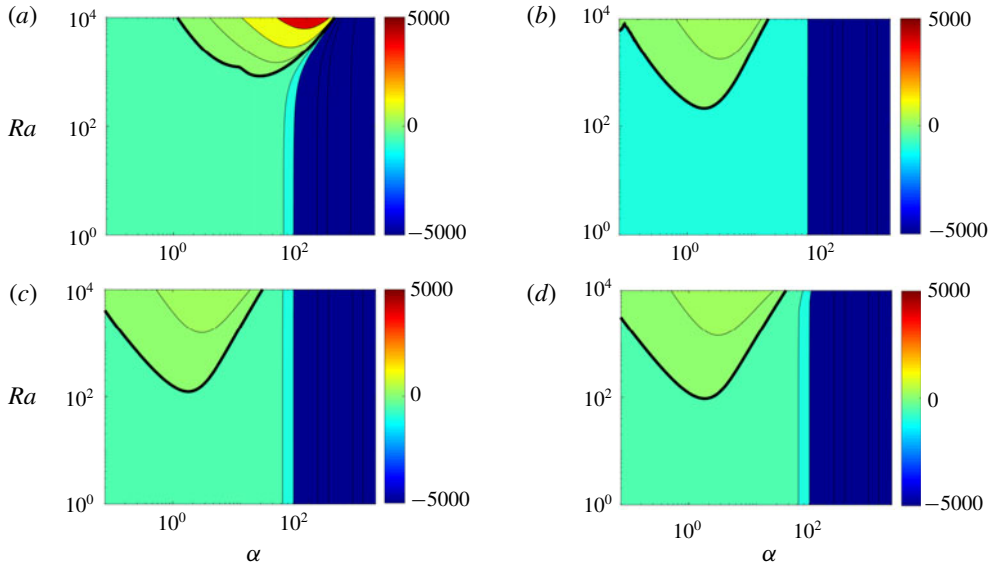

FIGURE 2. Contours of the growth rate ω_i of the most unstable mode in the Ra–α plane for $\beta = 0$: (*a*) $S_{max} = 0$; (*b*) $S_{max} = 11$; (*c*) $S_{max} = 20$; (*d*) $S_{max} = 30$.

damped, while the low-wavenumber region ($\alpha < 20$) is destabilised (figure 2*b–d*). This tendency observed with increasing maximum base-flow vorticity is fairly similar to that in the uniform shear flow (Hwang & Pedley 2014*a*). However, it should be mentioned in that case, even the low-wavenumber region was also found to be completely stabilised once $S_{max} > S_s$, whereas, in the present study, the region remains unstable even when S_{max} is roughly three times greater than S_s. Qualitatively, the same feature appears for the streamwise uniform instability mode ($\alpha = 0$), as shown in figure 3. The only difference between this case and the spanwise uniform case is that the streamwise uniform mode exhibits higher growth rates at low spanwise wavenumbers ($\beta < 20$) as S_{max} increases.

3.3. *Physical mechanism of the instability*

To understand the origin of the persistent instability, even at a considerably large base-flow vorticity, we first explore how the basic-state cell-number density profile is correlated with that of the eigenfunction of the instability mode. Figure 4 shows the basic-state cell-number density (*a,c,e,g*) and the cross-streamwise structure of the most unstable eigenmode (*b,d,f,h*) for $\alpha = 0$, $\beta = 10$ and $Ra = 2000$. As explained previously, the maximum n_0, which indicates the position of the cell layer formed by the gyrotactic trapping, shifts downwards with increasing S_{max}. Interestingly, the vertical location, in which the eigenmode appears in the form of counter-rotating rolls with the corresponding cell-number density field, also moves downwards together with the peak location of n_0. Furthermore, for all S_{max} considered here, the eigenmode of the instability consistently emerges in the region where the basic cell-number density is unstably stratified (i.e. $\mathrm{d}n_0/\mathrm{d}y > 0$), suggesting that the instability would be associated with the gravitational overturning mechanism observed in Rayleigh–Bénard convection and the Rayleigh–Taylor instability.

Downloaded from https://www.cambridge.org/core. Imperial College London Library, on 15 Apr 2019 at 13:41:41, subject to the Cambridge Core terms of use, available at https://www.cambridge.org/core/terms. https://doi.org/10.1017/jfm.2019.227

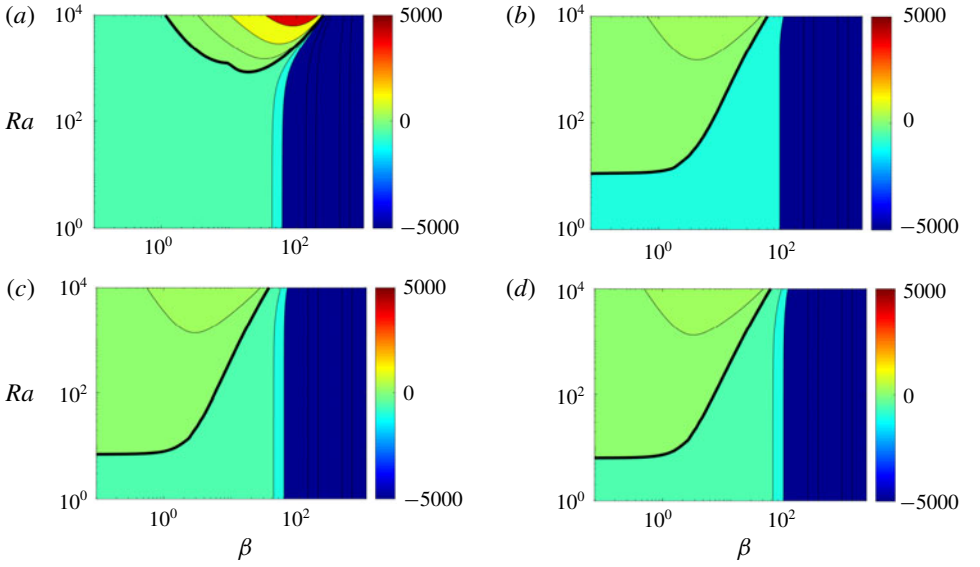

FIGURE 3. Contours of the growth rate ω_i of the most unstable mode in the Ra–β plane for $\alpha = 0$: (*a*) $S_{max} = 0$; (*b*) $S_{max} = 11$; (*c*) $S_{max} = 20$; (*d*) $S_{max} = 30$.

The precise mechanism of the instability persisting at large S_{max} is further investigated by carefully examining each term of (2.5). Four different physical mechanisms of instability are identified in the present case: (1) gravitational instability ($\mathcal{D}n_0$ in the third row of (2.5*a*)); (2) gyrotactic instability (all the terms with G_1 in (2.5*e*) and (2.5*f*)); (3) diffusion-oriented instability (all the terms with G_2 in (2.5*e*) and (2.5*f*)); (4) instability caused by the spatial gradient of cell-swimming vector field ($V_c\mathcal{D}\langle e_{20}\rangle_0$ in (2.5*d*)). The first three mechanisms here were previously shown to play almost equally important roles in bioconvection instability (Hwang & Pedley 2014*a*), while the last one was shown to be the central mechanism for the blip instability in downward channel flow (Hwang & Pedley 2014*b*). Given the scope of the present study for the instability of gyrotactic trapping, here we focus on the instability emerging for $S_{max} > S_s$. In such a case, the spanwise vorticity of the base flow would be fairly large in most of the vertical domain, and this yields all ξ_i in (2.5) fairly small (the values of ξ_i quickly diminish to zero as $S(y) \to \infty$; see figure 6 in Hwang & Pedley 2014*a*). We note that the ξ_i appear with G_1 and G_2 throughout (2.5), indicating that the gyrotactic and diffusion-oriented mechanisms are unlikely to be very active for $S_{max} > S_s$.

The discussion given above now suggests that the potential instability mechanism of the layer formed by gyrotactic trapping would originate from the gravitational mechanism and/or the one by the spatial gradient of cell-swimming vector field. To check this, we perform a numerical experiment for $Ra = 2000$ and $S_{max} = 20$, in which linear stability is examined by suppressing each of the terms discussed above individually. As shown in figure 5, the dominant contribution of the instability is made by the term associated with the gravitational mechanism (i.e. $\mathcal{D}n_0$ in the third row of (2.5*a*)), as its suppression leads to complete stabilisation. However, the one from the spatial gradient of cell-swimming vector field is found to play no role because its suppression hardly changes the growth rate, suggesting that the dominant instability mechanism in the present study is the gravitational one.

Downloaded from https://www.cambridge.org/core. Imperial College London Library, on 15 Apr 2019 at 13:41:41, subject to the Cambridge Core terms of use, available at https://www.cambridge.org/core/terms. https://doi.org/10.1017/jfm.2019.227

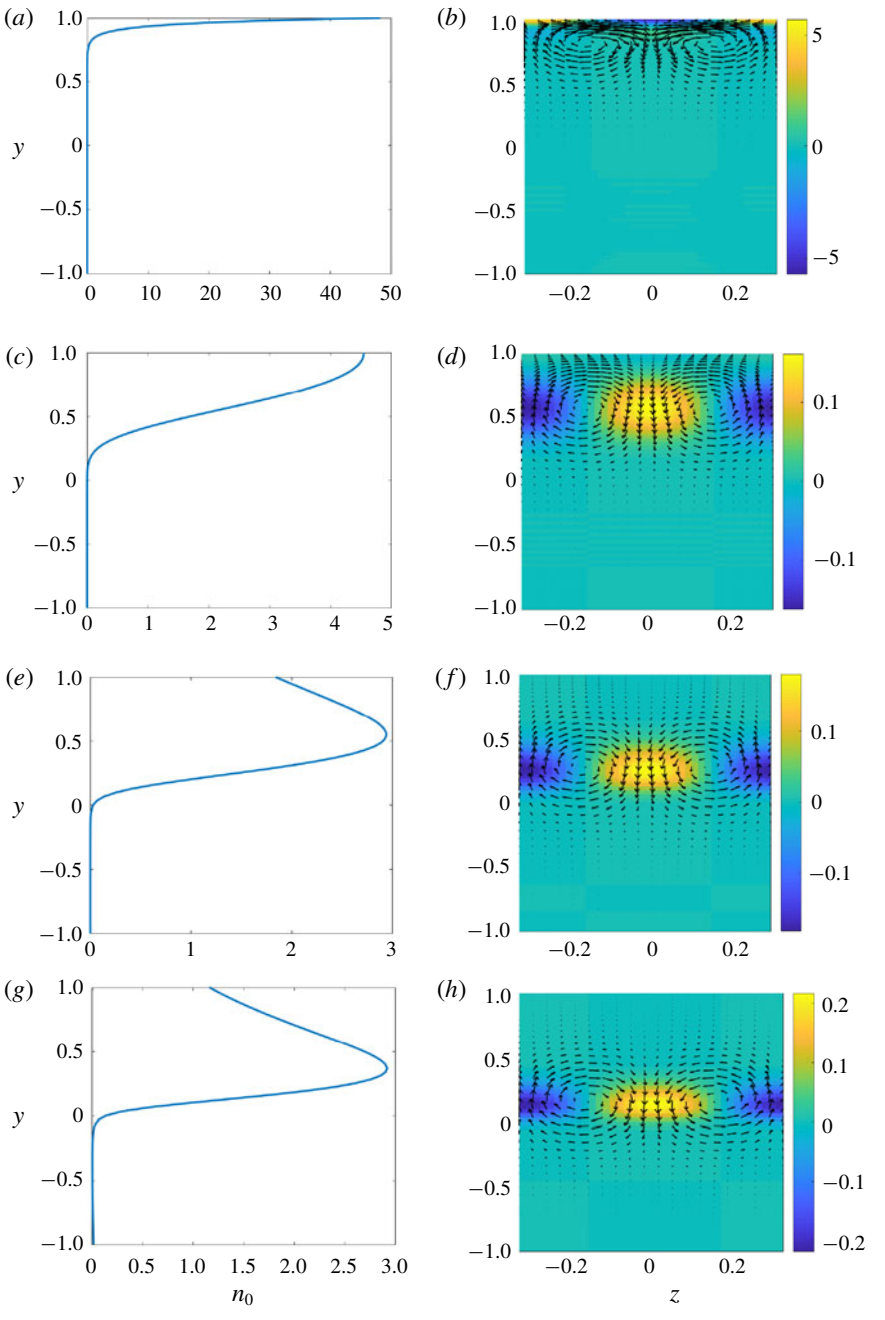

FIGURE 4. Basic-state cell-number density (*a,c,e,g*) and cross-streamwise view of the corresponding eigenfunction for $\alpha = 0$, $\beta = 10$ and $Ra = 2000$ (*b,d,f,h*): (*a,b*) $S_{max} = 0$; (*c,d*) $S_{max} = 11$; (*e,f*) $S_{max} = 20$; (*g,h*) $S_{max} = 30$. Here, the velocity vectors show the spanwise and wall-normal velocity perturbation, and the contours indicate the perturbed cell-number density. The velocity perturbation and the perturbed cell-number density are normalised by $-\max|\hat{v}||_{z=0}$.

Downloaded from https://www.cambridge.org/core. Imperial College London Library, on 15 Apr 2019 at 13:41:41, subject to the Cambridge Core terms of use, available at https://www.cambridge.org/core/terms.
https://doi.org/10.1017/jfm.2019.227

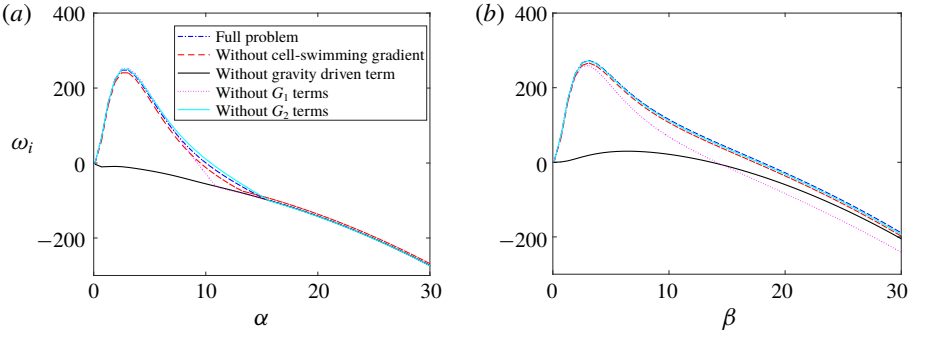

FIGURE 5. Examination of the instability mechanisms for $S_{max} = 20$ and $Ra = 2000$: (*a*) ω_i versus α with $\beta = 0$; (*b*) ω_i versus β with $\alpha = 0$.

4. Concluding remarks

Our study indicates that while a layer of bottom-heavy cells formed by gyrotactic trapping is indeed an equilibrium solution to the continuum equations describing such a suspension, this layer is also linearly unstable. The high shear rate ($S_{max} \geqslant 20$) critical Rayleigh number for this instability is two orders of magnitude lower than that for typical bioconvection. This implies that the gyrotactically trapped layer would be unstable at fairly low cell concentrations. In a suspension for the depth $d(= 2h) = 0.5$ cm, bioconvection occurs at $N \simeq 10^6$ cells cm^{-3}. Based on our results, a gyrotactically trapped layer would be unstable only at $N \simeq 10^4$ cells cm^{-3} for the same depth. It is interesting to note that this value of the cell concentration for the onset of the instability is fairly close to the $N \simeq 10^3$–10^4 cells cm^{-3} observed in thin layers at Monterey Bay (Jiménez *et al.* 1987; Steinbuck *et al.* 2009). As mentioned in the introduction, the thin layers of phytoplankton often develop in regions where turbulence is suppressed by strong density stratification (Dekshenieks *et al.* 2001). This suggests that the instability observed in the present study might be a mechanism that limits the cell concentration of thin layers in aqueous environments where turbulence is weak. The physical mechanism of this instability is also robust – as in bioconvection, it is a simple gravitational instability caused by the dense layer formed by gyrotactic trapping. Ecologically, it is unclear why the cells would exhibit such collective behaviour. However, this might be an evolutionary outcome that the cells have developed to prevent the development of high concentrations. High cell concentrations could lead to a competitive environment for nutrient uptake, and could weaken cell-swimming capabilities through hydrodynamic interactions between nearby cells, leaving the population susceptible to predators.

Despite this encouraging comparison, in the experiment of Durham *et al.* (2009), the formation of gyrotactically trapped cell layers was observed in a 'time-averaged' sense even for $N \simeq 10^6$ cells cm^{-3} (see figure 2*a* in Durham *et al.* 2009). In light of our current findings, this observation suggests the importance of the nonlinear evolution of the instability, especially as a function of the averaged cell-number density. It is certainly possible that the instability is not strong enough at low average cell-number densities (or Rayleigh numbers) to strongly disturb the layer formed by gyrotactic trapping. In other words, at low averaged cell-number densities, the relatively weak instability may give rise to unsteady layer dynamics (as was also confirmed by private communication with W. M. Durham) with an overall

Downloaded from https://www.cambridge.org/core. Imperial College London Library, on 15 Apr 2019 at 13:41:41, subject to the Cambridge Core terms of use, available at https://www.cambridge.org/core/terms.
https://doi.org/10.1017/jfm.2019.227

time-averaged shape. Notwithstanding, there may be a more intricate interplay between cellular gyrotaxis and the evolution of the cell-layer instability that can only be ascertained through an exploration of the fully nonlinear regime. This can probably be studied with classical weakly nonlinear stability analysis as well as with full-nonlinear simulations of the continuum model. Performing more extensive and carefully controlled experiments on this issue would also be highly desirable.

Finally, the typical thickness of the layer formed by gyrotactic trapping would be estimated by $l \sim D_v/V_c^*$. For *C. nivalis*, $l \sim O(0.1\text{–}1$ mm) (Pedley 2010, see also figure 1*a*) and the time scale of the instability would be greater than $O(1$ s) for $N < 10^6$ cells cm^{-3} (figure 5). We note that the typical Kolmogorov length and time scales in oceans are $\eta \sim O(0.1\text{–}10$ mm) and $\tau_\eta \sim O(0.1\text{–}10^2$ s) (Durham *et al.* 2013). This implies that turbulent mixing in oceans would easily disrupt the layer formation process as well as its instability, consistent with the observation by Dekshenieks *et al.* (2001). However, precisely to what extent and how this would happen needs to be understood. Other interesting avenues for further research would also include the role of hydrodynamic interactions as well as the effects of changes in the swimmers' physical properties (shape, distribution of mass, rigidity of the body). The hydrodynamic interactions between the cells can alter the precise shape of the layer, as they would impact on the diffusivity and rheology of the suspension (Ishikawa & Pedley 2007). The shape of the cell can also affect the dynamics of the suspension. For example, the layer may form at lower shear rates for elongated cells due to enhanced sedimentation by the vertical shear (Clifton, Bearon & Bees 2018). The instability for such a layer also deserves a future investigation.

Acknowledgements

We gratefully acknowledge Dr W. M. Durham, who kindly provides a detailed explanation on his early experimental observation (Durham *et al.* 2009). We are grateful to the anonymous referees of this paper for their constructive comments on the original manuscript.

References

Bees, M. & Hill, N. 1997 Wavelengths of bioconvection patterns. *J. Expl Biol.* **200** (10), 1515–1526.

Bees, M. A. & Hill, N. A. 1998 Linear bioconvection in a suspension of randomly swimming, gyrotactic micro-organisms. *Phys. Fluids* **10** (8), 1864–1881.

Clifton, W., Bearon, R. N. & Bees, M. A. 2018 Enhanced sedimentation of elongated plankton in simple flows. *IMA J. Appl. Maths* **83** (4), 743–766.

Croze, O. A., Ashraf, E. E. & Bees, M. A. 2010 Sheared bioconvection in a horizontal tube. *Phys. Biol.* **7** (4), 046001.

Dekshenieks, M. M., Donaghay, P. L., Sullivan, J. M., Rines, J. E. B., Osborn, T. R. & Twardowski, M. S. 2001 Temporal and spatial occurrence of thin phytoplankton layers in relation to physical processes. *Mar. Ecol. Prog. Ser.* **223**, 61–71.

Durham, W. M., Clement, E., Berry, M., Lillio, F., De Boffetta, G., Cencini, M. & Stocker, R. 2013 Turbulence drives microscale patches of motile phytoplankton. *Nat. Comm.* **4**, 2148.

Durham, W. M., Kessler, J. O. & Stocker, R. 2009 Disruption of vertical motility by shear triggers formation of thin phytoplankton layers. *Science* **323** (5917), 1067–1070.

Durham, W. M. & Stocker, R. 2012 Thin phytoplankton layers: characteristics, mechanisms, and consequences. *Annu. Rev. Marine Sci.* **4**, 177–207.

Franks, P. J. S. 1995 Thin layers of phytoplankton: a model of formation by near-inertial wave shear. *Deep-Sea Res.* I **42** (1), 75–91.

Ginzburg, M. & Ginzburg, B. Z. 1985 Influence of age of culture and light intensity on solute concentrations in two *Dunaliella* strains. *J. Exp. Botany* **36** (5), 701–712.

Downloaded from https://www.cambridge.org/core. Imperial College London Library, on 15 Apr 2019 at 13:41:41, subject to the Cambridge Core terms of use, available at https://www.cambridge.org/core/terms. https://doi.org/10.1017/jfm.2019.227

GRÜNBAUM, D. 2009 Peter principle packs a peck of phytoplankton. *Science* **323** (5917), 1022–1023.

HILL, N. A. & BEES, M. A. 2002 Taylor dispersion of gyrotactic swimming micro-organisms in a linear flow. *Phys. Fluids* **14** (8), 2598–2605.

HWANG, Y. & PEDLEY, T. J. 2014*a* Bioconvection under uniform shear: linear stability analysis. *J. Fluid Mech.* **738**, 522–562.

HWANG, Y. & PEDLEY, T. J. 2014*b* Stability of downflowing gyrotactic microorganism suspensions in a two-dimensional vertical channel. *J. Fluid Mech.* **749**, 750–777.

ISHIKAWA, T. & PEDLEY, T. J. 2007 The rheology of a semi-dilute suspension of swimming model micro-organisms. *J. Fluid Mech.* **588**, 399–435.

JIMÉNEZ, F., RODRÍGUEZ, J., BAUTISTA, B. & RODRÍGUEZ, V. 1987 Relations between chlorophyll, phytoplankton cell abundance and biovolume during a winter bloom in Mediterranean coastal waters. *J. Exp. Mar. Bio. Ecol.* **105** (2–3), 161–173.

JOHNSTON, T. M. S. & RUDNICK, D. L. 2009 Observations of the transition layer. *J. Phys. Oceanogr.* **39** (3), 780–797.

KESSLER, J. O. 1984 Gyrotactic buoyant convection and spontaneous pattern formation in algal cell cultures. In *Nonequilibrium Cooperative Phenomena in Physics and Related Fields*, pp. 241–248. Springer.

KESSLER, J. O. 1985 Hydrodynamic focusing of motile algal cells. *Nature* **313** (5999), 218–220.

KRIVTSOV, V., BELLINGER, E. G. & SIGEE, D. C. 2000 Changes in the elemental composition of *Asterionella formosa* during the diatom spring bloom. *J. Plankton Res.* **22** (1), 169–184.

MACINTYRE, J. G., CULLEN, J. J. & CEMBELLA, A. D. 1997 Vertical migration, nutrition and toxicity in the dinoflagellate *Alexandrium tamarense*. *Mar. Ecol. Prog. Ser.* **148**, 201–216.

MOLINE, M. A., BENOIT-BIRD, K. J., ROBBINS, I. C., SCHROTH-MILLER, M., WALUK, C. M. & ZELENKE, B. 2010 Integrated measurements of acoustical and optical thin layers II: horizontal length scales. *Cont. Shelf Res.* **30** (1), 29–38.

NIELSEN, T. G., KIØRBOE, T. & BJØRNSEN, P. K. 1990 Effects of a *Chrysochromulina polylepis* subsurface bloom on the planktonic community. *Mar. Ecol. Prog. Ser.* **62**, 21–35.

OSBORN, T. 1998 Finestructure, microstructure, and thin layers. *Oceanography* **11**, 36–43.

PEDLEY, T. J. 2010 Instability of uniform micro-organism suspensions revisited. *J. Fluid Mech.* **647**, 335–359.

PEDLEY, T. J., HILL, N. A. & KESSLER, J. O. 1988 The growth of bioconvection patterns in a uniform suspension of gyrotactic micro-organisms. *J. Fluid Mech.* **195**, 223–237.

PEDLEY, T. J. & KESSLER, J. O. 1987 The orientation of spheroidal microorganisms swimming in a flow field. *Proc. R. Soc. Lond.* B **231** (1262), 47–70.

PEDLEY, T. J. & KESSLER, J. O. 1990 A new continuum model for suspensions of gyrotactic micro-organisms. *J. Fluid Mech.* **212**, 155–182.

PEDLEY, T. J. & KESSLER, J. O. 1992 Hydrodynamic phenomena in suspensions of swimming microorganisms. *Annu. Rev. Fluid Mech.* **24** (1), 313–358.

RUSCONI, R., GUASTO, J. S. & STOCKER, R. 2014 Bacterial transport suppressed by fluid shear. *Nat. Phys.* **10** (3), 212–217.

RYAN, J. P., MCMANUS, M. A. & SULLIVAN, J. M. 2010 Interacting physical, chemical and biological forcing of phytoplankton thin-layer variability in Monterey Bay, California. *Cont. Shelf Res.* **30** (1), 7–16.

SANTAMARIA, F., DE LILLO, F., CENCINI, M. & BOFFETTA, G. 2014 Gyrotactic trapping in laminar and turbulent Kolmogorov flow. *Phys. Fluids* **26** (11), 111901.

SIMILÄ, A. 1988 Spring development of a chlamydomonas population in Lake Nimetön, a small humic forest lake in southern Finland. In *Flagellates in Freshwater Ecosystems*, pp. 149–157. Springer.

STACEY, M. T., MCMANUS, M. A. & STEINBUCK, J. V. 2007 Convergences and divergences and thin layer formation and maintenance. *Limnol. Oceanogr.* **52** (4), 1523–1532.

STEINBUCK, J. V., STACEY, M. T., MCMANUS, M. A., CHERITON, O. M. & RYAN, J. P. 2009 Observations of turbulent mixing in a phytoplankton thin layer: implications for formation, maintenance, and breakdown. *Limnol. Oceanogr.* **54** (4), 1353–1368.

SULLIVAN, J. M., DONAGHAY, P. L. & RINES, J. E. B. 2010 Coastal thin layer dynamics: consequences to biology and optics. *Cont. Shelf Res.* **30** (1), 50–65.

Downloaded from https://www.cambridge.org/core. Imperial College London Library, on 15 Apr 2019 at 13:41:41, subject to the Cambridge Core terms of use, available at https://www.cambridge.org/core/terms. https://doi.org/10.1017/jfm.2019.227